Pressure Distribution Behind a Nonstationary Reflected-Diffracted Oblique Shock Wave

R. S. Srivastava* and R. L. Deschambault†
University of Toronto, Ontario, Canada

THE behavior of the pressure distribution behind a nonstationary reflected-diffracted oblique shock wave over a 5.7 deg sharp corner, moving at a shock Mach number of 1.39, was obtained experimentally using infinite fringe interferometric techniques. The results agree well with previous analytical predictions.

Lighthill[1] obtained the pressure distribution along a wedge surface after a normal shock wave had undergone diffraction past a small sharp expansion corner. Fletcher et al.[2] conducted experiments in a shock tube in order to test the analysis by Lighthill. The densities in the diffracted flow were measured interferometrically. Due to the small deflection, pressures could be obtained from the densities by using the isentropic equation of state.

The analogous problem of a plane shock wave hitting an inclined wall and the resulting reflected shock-wave pattern diffracting past a sharp corner was considered by Srivastava[3] and Srivastava and Chopra.[4] Srivastava[3] developed an analysis based on Lighthill's approach and treated the cases when the relative outflow behind the reflected shock before diffraction was both subsonic and sonic. Subsequently, Srivastava and Chopra[4] considered the case when the relative outflow behind the reflected shock wave before diffraction as supersonic.

Experiments were conducted in the UTIAS 10×18 cm Hypervelocity Shock Tube to investigate the densities in the diffracted flow behind a reflected-diffracted shock wave past a sharp corner. Figure 1 illustrates the schematic diagram of the incident shock wave I, the various thermodynamic states (0-5), and the geometry of the wedge. Initially the incident shock was allowed to strike a wedge of 70 deg to produce a regular reflection configuration. The configuration was then allowed to pass over a sharp corner angle of $\delta=5.7$ deg, at point B in Fig. 2. The sharp expansion corner angle δ provided the necessary condition for the diffraction of the regular reflection pattern. The incident shock wave was moving at a Mach number $M_s=1.39$, into air initially at a pressure of 750.5 Torr and a temperature of 298.5 K. The uniform and disturbed regions and their constant density lines (isopycnics) are clearly shown in the infinite fringe interferogram in Fig. 2. Four uniform regions (0-3) and two nonuniform regions (4, 5) are generated. The analysis by Srivastava and Chopra[4] dealt with the four uniform regions and with only one nonuniform region, (4). Region (4) is produced when the signal from the corner at point B in Fig. 2 propagates into states (2) and (3) with a sonic circle bounded by states (4) (a) and (4) (l). The other nonuniform region, (5), is produced when the signal from the first compressive corner propagates into the flow behind the reflected shock until it reaches state (2). This region behind the detached bow wave was not considered in the original analysis. Hence, five of the observed regions after diffraction agree with the predictions given by Srivastava and Chopra.[4]

The density distribution of the flow field was obtained using a 23-cm-diam Mach-Zehnder interferometer in the infinite fringe mode. The density in the uniform region (3) immediately behind the reflected shock, which can readily be calculated, was used as a reference. The evaluation of the density field is shown in Table 1 and was obtained in the usual manner.[5]

The pressure distribution over the wedge surface was obtained from the experimental density distribution by assuming the isentropic equation of state $p=A\rho\gamma$, where p is the pressure, ρ the density, γ the ratio of specific heats, and A a constant to be determined from the initial parameters. The experimental and analytical results are compared in Fig. 3. Also, in Fig. 3, the relative deficiency of pressure at the wall in regions (3) and (4) divided by the corner angle δ in radians has been plotted against the distance coordinate x. The distances along the wedge surface were normalized by the original surface distance AB from the shock wave to the corner at point B. In this scheme, the sharp expansion corner δ occurs at $x=1$. In the analysis a mathematical singularity exists at the corner, point B. As expected a finite pressure is measured at the corner experimentally, as shown in Fig. 3. The analytic shock Mach number of 1.36 was slightly lower than the experimental value of 1.39. However, the results are in good agreement despite this small difference.

The need for accurate analytical and numerical descriptions of oblique-shock-wave reflections and the associated properties of the flowfields cannot be overemphasized. Problems such as the transition from regular to Mach reflection and the structure of the isopycnics resulting from the reflection of a normal shock from compressive corners, just to name two, can benefit greatly from an enhanced understanding of the entire flowfield (see Deschambault and Glass[6]).

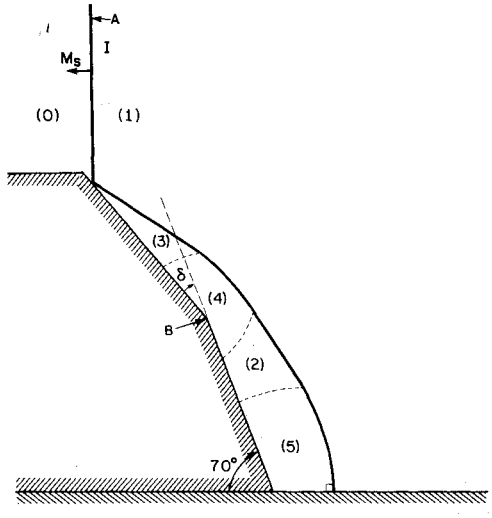

Fig. 1 Schematic diagram of the shock reflection pattern after diffraction.

Table 1 Evaluation of the density field

Region	ρ/ρ_0	Region	ρ/ρ_0
(0)	0.382	(4) (e)	0.975
(1)	0.637	(f)	0.970
(2)	1.002	(g)	0.975
(3)	1.000	(h)	0.980
(4) (a)	0.995	(i)	0.985
(b)	0.990	(j)	0.990
(c)	0.985	(k)	0.995
(d)	0.980	(l)	1.000

Received Oct. 20, 1982; revision received March 15, 1983.

*Visiting Scientist, Department of Aerospace Science and Engineering; Deputy Chief Scientific Officer, on leave from Defence Science Center, Metcalfe House, Delhi, India.

†Research Associate, Department of Aerospace Science and Engineering, Institute for Aerospace Studies.

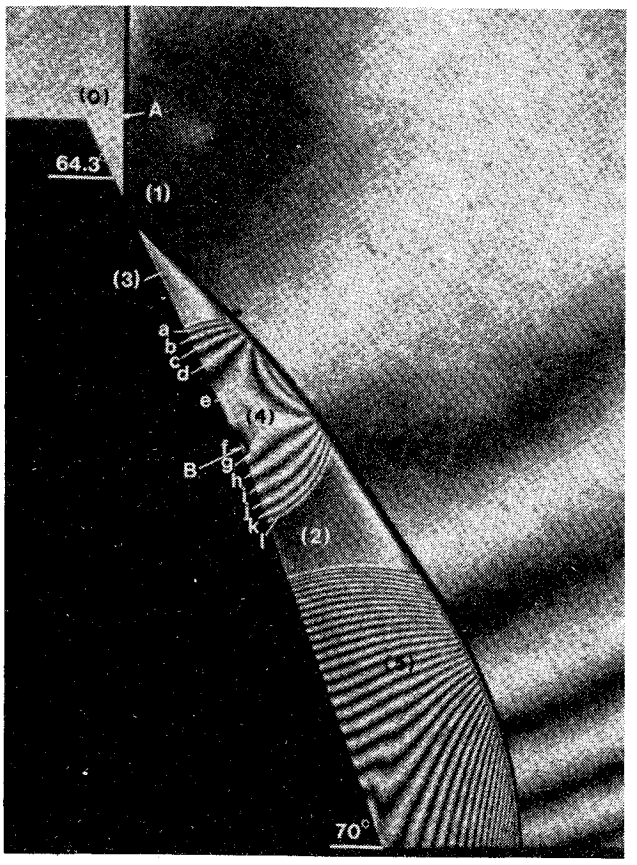

Fig. 2 Infinite fringe interferogram in air. $M_s = 1.39$; $\theta_w = 70$ deg; $p_0 = 750.5$ Torr; $\rho_0 = 0.116 \times 10^{-2}$ g/cm^3; $T_0 = 298.5$ K; $M_2 = 0.26$; $p_2 = 2980$ Torr; $\rho_2 = 0.306 \times 10^{-2}$ g/cm^3; $T_2 = 453$ K; $u_2 = 112.6$ m/s; $M_3 = 0.30$; $p_3 = 2964$ Torr; $\rho_3 = 0.305 \times 10^{-2}$ g/cm^3; $T_3 = 453$ K; $u_3 = 128.7$ m/s; taken at a wavelength of $\lambda = 3471.5$ Å. (u_i stands for the particle velocity in state (i).)

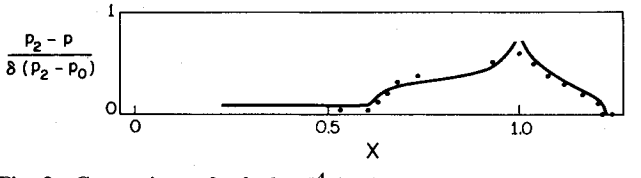

Fig. 3 Comparison of calculated[4] (—) and measured (●) relative pressure deficiency along the surface of the wedge.

Acknowledgments

The authors appreciate the invaluable guidance received from Prof. I. I. Glass. The fruitful discussions with Dr. J. J. Gottlieb are gratefully acknowledged. The first author wishes to thank the Defence Research and Development Organization, New Delhi, India, for support during his sabbatical leave at UTIAS. The financial support received from the Defence Research Establishment Suffield, Ralston, Alberta, Canada and the U.S. Air Force under grant AF-AFOSR 82-0096 is acknowledged with thanks.

References

[1]Lighthill, M. J., "The Diffraction of Blast. I," *Proceedings of the Royal Society of London*, Ser. A, Vol. 198, 1949, pp. 454-470.

[2]Fletcher, C. H., Weimer, D. K., and Bleakney, W., "Pressure behind a Shock Wave Diffracted through a Small Angle," *Physical Review*, Vol. 78, No. 5, 1950, pp. 634-635.

[3]Srivastava, R. S., "Diffraction of Blast Waves for the Oblique Case," British Aeronautical Research Council Current Papers, No. 1008, 1968.

[4]Srivastava, R. S. and Chopra, M. G., "Diffraction of Blast Waves for the Oblique Case," *Journal of Fluid Mechanics*, Vol. 40, Pt. 4, 1970, pp. 821-831.

[5]Ando, S., "Pseudo-Stationary Oblique Shock-Wave Reflection in Carbon Dioxide-Domains and Boundaries," University of Toronto, UTIAS TN 231, 1981.

[6]Deschambault, R. L. and Glass, I. I., "An Update on Non-stationary Oblique-Shock-Wave Reflections: Actual Isopycnics and Numerical Experiments," *Journal of Fluid Mechanics*, Vol. 131, 1983, pp. 27-57.

Balance of Turbulent Energy in the Linear Wall Region of Channel Flow

Peter S. Bernard* and Bruce S. Berger†
University of Maryland, College Park, Maryland

Introduction

A DESCRIPTION of the energy balance in the wall region of turbulent flow is of importance both in understanding the physical processes of turbulent motion and in developing useful closure models.[1] Laufer[2] experimentally determined an energy budget for turbulent pipe flow. Some of the terms in the energy equation were found directly using hot wire probes. Others, in the dissipation term, were obtained using Taylor's hypothesis and the assumption of isotropy; while the term containing pressure was found as the closing entry. Later Townsend[3] corrected Laufer's estimates of the dissipation term and deduced the energy balance given in Fig. 1. The validity of these curves, for small y^+, has not been established conclusively, owing to the breakdown of Taylor's hypothesis and the isotropy assumptions in this region.

Eckelmann[4] and Kreplin and Eckelmann[5] made a detailed study of turbulent oil channel flow with a large viscous sublayer for small y^+ using a hot-film probe and a flush mounted hot-film wall element. In particular, Eckelmann[4] discovered that the rms streamwise and transverse velocities u' and w', respectively, were proportional to y^+ only for a thin region $0 \leq y^+ \lesssim 0.1$, which he termed the viscous wall layer. In the present Note it is shown that the presence of a very small viscous wall layer is in contradiction with the energy balance in Fig. 1, for at least $0 \leq y^+ \lesssim 2$, if it is assumed that channel and pipe flows have a similar energy balance in this region.

Turbulent Kinetic Energy Equation

The turbulent kinetic energy equation for fully developed turbulent channel flow is[6]

$$0 = \underbrace{-\langle uv\rangle \frac{\partial U}{\partial y}}_{\text{P}} + \underbrace{\frac{\nu}{2}\frac{\partial^2}{\partial y^2}\left(\langle u^2\rangle + \langle v^2\rangle + \langle w^2\rangle\right)}_{\text{GD}} \underbrace{-\frac{1}{\rho}\frac{\partial}{\partial y}\langle pv\rangle}_{\text{PD}}$$
$$-\nu\left(\left\langle\left(\frac{\partial u}{\partial x}\right)^2\right\rangle + \left\langle\left(\frac{\partial v}{\partial x}\right)^2\right\rangle + \left\langle\left(\frac{\partial w}{\partial x}\right)^2\right\rangle\right.$$
$$\underbrace{+\left\langle\left(\frac{\partial u}{\partial y}\right)^2\right\rangle + \left\langle\left(\frac{\partial v}{\partial y}\right)^2\right\rangle + \left\langle\left(\frac{\partial w}{\partial y}\right)^2\right\rangle + \left\langle\left(\frac{\partial u}{\partial z}\right)^2\right\rangle}_{\text{D}}$$
$$\left.+\left\langle\left(\frac{\partial v}{\partial z}\right)^2\right\rangle + \left\langle\left(\frac{\partial w}{\partial z}\right)^2\right\rangle\right) \underbrace{-\frac{1}{2}\frac{\partial}{\partial y}\left(\langle vu^2\rangle + \langle v^3\rangle + \langle vw^2\rangle\right)}_{\text{KD}} \tag{1}$$

Received March 29, 1982; revision received Sept. 20, 1982.

*Associate Professor, Dept. of Mechanical Engineering.
†Professor, Dept. of Mechanical Engineering.